Kinetics of the reduction of hematite (Fe_2O_3) by methane (CH_4) during chemical looping combustion: a global mechanism

Esmail R. Monazam[2], Ronald W. Breault[*1], Ranjani Siriwardane[1], George Richards[1], and Stephen Carpenter[3]

[1]National Energy Technology Laboratory
U. S. Department of Energy
3610 Collins Ferry Rd.
Morgantown, West Virginia 26507-0880
[2]REM Engineering Services, PLLC
3537 Collins Ferry Rd.
Morgantown, West Virginia 26505
[3]URS Energy & Construction, Inc.
3610 Collins Ferry Rd.
Morgantown, WV. 26505

Abstract

Chemical-looping combustion (CLC) has emerged as a promising technology for fossil fuel combustion which produces a sequestration ready concentrated CO_2 stream in power production. A CLC system is composed with two reactors, an air and a fuel reactor. An oxygen carrier such as hematite (94%Fe_2O_3) circulates between the reactors, which transfers the oxygen necessary for the fuel combustion from the air to the fuel. An important issue for the CLC process is the selection of metal oxide as oxygen carrier, since it must retain its reactivity through many cycles. The primary objective of this work is to develop a global mechanism with respective kinetics rate parameters such that CFD simulations can be performed for large systems. In this study, thermogravimetric analysis (TGA) of the reduction of hematite (Fe_2O_3) in a continuous stream of CH_4 (15, 20, and 35%) was conducted at temperatures ranging from 700 to 825 ^oC over ten reduction cycles. The mass spectroscopy analysis of product gas indicated the presence of CO_2 and H_2O at the early stage of reaction and H_2 and CO at the final stage of reactions. A kinetic model based on two parallel reactions, 1) first-order irreversible rate kinetics and 2) Avrami equation describing nucleation and growth processes, was applied to the reduction data. It was found, that the reaction rates for both reactions increase with, both, temperature and the methane concentration in inlet gas.

Introduction

The increase in the CO_2 concentration, a major green house gas, in the atmosphere due to the combustion of fossil fuels such as coal, petroleum, and natural gas may lead to disastrous changes in our planet's climate. The concentration of CO_2 in the atmosphere

* Corresponding author: Tel. 304-285-4486; fax:304-285-4403; email: Ronald.breault@netl.doe.gov

has risen to a value of ~370 ppm today, from the preindustrial value of 280 ppm[1]. Since historic levels of CO_2 have been both higher and lower than these levels, a direct link to anthropogenic actions is not possible. Even so, it is adventitious to look for ways to reduce and control the anthropogenic contribution. At present, there are a number of CO_2 capture processes[2] capable of doing this, (1) precombustion, in which the hydrocarbon fuels are decarbonized prior to combustion; (2) oxyfuel combustion, which uses pure oxygen separated from air; and (3) post combustion separation, which separates CO_2 from the flues gases using different methods. All of these techniques have high costs and large energy penalty, resulting in a significant decrease (9-27 %) of the overall combustion efficiency and a price increase (1.2 - 2.3 times) of the energy[3-5]. An alternative process such as chemical-looping combustion (CLC) has been proposed for the reduction of CO_2 emissions[6, 7].

Chemical looping combustion (CLC) is a novel process for heat and power production with inherent CO_2 separation[8–10]. An oxygen carrier such as Fe_2O_3, CuO and NiO performs the task of transferring oxygen from air for the combustion of fuel[11]. Generally, these metal oxides are combined with an inert material such as Al_2O_3, ZrO_2, TiO_2 , SiO_2, $MgAl_2O_4$, $NiAl_2O_4$, and bentonite which acts as a porous support providing a higher surface area for reaction, and as a binder for increasing the mechanical strength and attrition resistance[12] of these oxygen carrying solids.

The CLC uses two reactors in the form of interconnected reactor beds (1) a fuel reactor where the metal oxide particles are reduced by reaction with the fuel, and (2) an air reactor where the reduced metal oxide from the fuel reactor is oxidized with air. The advantage with the technique compared to normal combustion is that the outlet gas from the fuel reactor consists of only CO_2 and H_2O, and thus no extra energy is needed for CO_2 separation. Extensive research on chemical looping combustion has been performed over the past decade at Korea Institute of Energy Research,[13,14] Tokyo Institute of Technology in Japan, [15–21] TDA Inc.,[22,23] Chalmers University of Technology in Göteborg[2], Sweden[2], CSIC in Zaragoza[2], Spain[19], U.S. Department of Energy (DOE)[23], University of Cambridge[24], and University of Colorado[25].

Fuel such as coal, biomass and natural gas are being used for reduction of the metal oxides in CLC. When methane is used as a reducing agent CO_2 emission are less compared to other fuels and contamination emissions are negligible. Also, among the fossil fuels on the earth, methane is one of the most abundant fuels both underground and in ocean as methane hydrates. In this study, methane is used as a reducing agent.

Among the metal oxides which are used as an oxygen carrier in CLC, iron oxide (Fe_2O_3) is very attractive one for commercial CLC application since it is relatively inexpensive, readily available as natural mineral sand also environmentally safe compared to other metal oxide such as NiO and CuO[26]. Research on CLC has so far mainly been focused on the development and selection of suitable oxygen carrier materials and the implementation of this concept in pilot scale tests. However, few studies reported in the literature have been focused on the determination of kinetic parameters of Fe_2O_3 based oxygen carriers. The knowledge of the kinetics data is of great importance in the design

of a CLC process, because it determines the solid inventory necessary in the fuel and air reactors, as well as the recirculation rate of oxygen carriers between the reactors. Many researchers have tried to develop a universal kinetic equation for gaseous reduction of iron oxides. However, it was only possible to obtain a set of independent equations, useful for the description of the reduction process within a certain range of reaction conditions[27-29].

One of the most important parameters of the hematite reduction is the apparent activation energy as it defines the reactor dimensions and the energy consumption. Literature survey indicates that its value depends on many factors such as chemical structure of the starting raw material, nature of reducing gas, temperature range, reaction step, presence of water vapor and other gases in the gas mixture, etc. The literature data suggests that activation energy obtained by reducing iron oxides with methane varies from 49-271 kJ/mole[30-32]. This wide range of value is due to the variation in rate controlling step assumed in developing the kinetic rates. Moreover, it is clear that the rate controlling mechanism is related to the many factors such as chemical and physical nature of starting raw material, gas composition and temperature range, etc.

Ghose et. al.[33] measured the rate reduction of porous and dense spherical pellets of iron oxide (Fe_2O_3) with 100% methane in the temperature range of 800−1025 ^oC. They suggested that the chemical reaction of Fe_2O_3 with CH_4 takes place in two steps:
1) Decomposition of methane into carbon and hydrogen;

$$CH_4(g) = C(s) + 2H_2(g) \quad (1)$$

2) Reduction of iron oxide by hydrogen;

$$H_2(g) + [O] = H_2O(g) \quad (2)$$

where [O] is the oxygen in iron oxide. Therefore, the overall reaction rate was considered as;

$$CH_4(g) + 2[O] = 2C(s)+2H_2O(g) \quad (3)$$

The apparent activation energy was obtained as 206 kJ/mole in the temperature range of 800-950 ^oC and 105.7 kJ/mole in the temperature range of 950-1025 ^oC for reaction (1) above. Furthermore, they claimed most of this apparent value was due to increase of concentration of hydrogen with increase in temperature due to enhanced cracking of CH_4. The primary difference of our work from the work by Ghose[33] is that we have investigated the reaction of CH_4 with iron oxide at different CH_4 concentrations (15-35%) and also we have extended the temperature to a lower rang of 700-825 ^oC.

The objective of this paper is to determine the kinetics parameters of the reduction reactions of Fe-based oxygen carriers, using CH_4. The effects of temperature (700-825 ^oC), flow rate, sample size, and methane concentration (15-35 %) were evaluated.

Experimental

Thermogravimetric Analysis (TGA) Apparatus

A sketch of the reactor unit a TA Model 2050 thermo gravimetric analyzer, is shown in Figure 1. A sample is placed on the pan which is centered in the gas feed and gas exit ports. The port at the bottom is closed. Sweep gas keeps the balance electronics in an inert environment and enters the reaction chamber at the top. A typical TGA experimental data on weight changes during reduction/oxidation for cyclic tests at a given temperature are illustrated in Figure 2. The samples were placed in a 5-mm deep and 10-mm diameter quartz crucible. For a typical test, about 60 mg of the hematite sample was heated in a quartz bowl at a heating rate of 15 °C/min in zero-grade air to the reaction temperature. The reduction−oxidation cycles were conducted within the temperature range 700−825 °C for 10 cycles, using 15%, 20%, and 35% CH_4 concentrations in N_2 for the reduction segment and in zero-grade air for the oxidation segment. The system was flushed with ultra-high pure nitrogen for 10 minutes before and after each reaction segment. The concentrations of CH_4, CO_2, H_2O, H_2, CO, and O_2 from the exit gas stream of the reactor were analyzed using a mass spectrometer. The mass spectrometer is manufactured by Pfeiffer Omnistar GSD-301. All experiments are carried out with a reaction gas flow rate of 45 sccm. Reduction reaction times were set at 45 min, and oxidation reaction times were 30 min for all experiments. The analysis arriving at these conditions and showing that there is no mass transfer or mixing issues confounding the analysis is presented in the Supplemental Information available online with the paper.

Test Matrix

Thermogravimetric reduction tests were carried out on commercial hematite particles originating from Wabush Mine, Canada. The chemical analysis of the hematite particle is given in Table 1. The hematite content of the material was 94% and the raw material was crushed in a lab to 60-100 μm with an average size of 80 μm. To examine the fundamental kinetics of the hematite conversions and the rate of CH_4 uptake information, experiments were carried out using a TA Model 2050 thermogravimetric analyzer.

Results and Discussion

The degree of conversion for reduction is defined as;

$$X = \frac{m_o - m(t)}{m_o - m_f} \qquad (4)$$

where $m(t)$ is the instantaneous weight of the solid during the exposure to CH_4. Parameters m_o and m_f are initial and final weight of the sorbent, respectively. In this study, the initial weight was considered as the weight of hematite and final weight as the weight of either Fe_3O_4, or FeO and or Fe (depends on degree of reductions). Therefore,

the kinetics of hematite reduction process was determined by monitoring the weight changes sustained by the specimen during the course of its reduction under isothermal conditions. Figure 3 illustrates the degree of reduction as a function of time obtained at different temperatures with 20 % CH_4. It can be clearly seen that the reaction rate is affected by the temperature. It should be noted that only 40 chosen data points are shown at each temperature for clear illustration of the trend of the curves in Figure 3. The solid lines represent the model fit to experimental data that will be discussed later.

The net weight change during reduction with CH_4 is due to oxygen removal and carbon deposition. Carbon contents in reduced hematite are illustrated by Figure 4. The amount of carbon deposition increased with increasing temperature and CH_4 concentration. The carbon contents were obtained using production of CO_2 in the oxidation process (Figure 5). The carbon content was obtained by integration of the area under the curves shown in Figure 5 and subtracted from and normalized by the total carbon fed to the reactor as CH_4. The carbon deposition mass was assumed to be deposited evenly over the 45 min reduction cycle and subtracted from the weight versus time data from the TGA. This had a insignificant effect on the results.

To determine the kinetic parameters of the hematite reduction reaction with methane, several experiments were conducted at different temperatures (700-825 ^oC) and concentrations (15%, 20%, and 35%). Considering the following series of reactions for hematite reduction:

$$Fe_2O_3 \rightarrow Fe_3O_4 \rightarrow FeO \rightarrow Fe \qquad (5)$$

The theoretically weight changes in accordance to reaction stoichiometry for CH_4 gas reduction of hematite were calculated according to the reaction listed below:

$$12Fe_2O_3 + CH_4 \rightarrow 8Fe_3O_4 + CO_2 + 2H_2O \qquad (6)$$

$$4Fe_2O_3 + CH4 \rightarrow 8FeO + CO_2 + 2H_2O \qquad (7)$$

and

$$4Fe_2O_3 + 3CH4 \rightarrow 8Fe + 3CO_2 + 6H_2O \qquad (8)$$

It was thus determined that the theoretical weight decrease corresponding to transformation of Fe_2O_3 into Fe_3O_4 is 3.3 wt %. Transformation of Fe_2O_3 into FeO and Fe corresponds to weight decrease of 10 wt% and 30 wt% respectively. In this study, m_f is considered as the mass of FeO and 100% conversion means that the hematite was all converted to FeO (wüsite).

One of the purposes of kinetic studies is to find the most probable series of reactions corresponding to the data in order to deduce the reaction mechanism. It is usual to postulate a model for reaction based on the rate-determining step. Therefore, attempts were made to fit the reduction of hematite data over the complete conversion range with suitable rate expressions derived from existing models for reduction, including those

reaction models listed in Table 2. These different rate models were examined to fit the TGA experimental data for the hematite/methane reduction reaction.

Kinetic Models

Kinetic analysis of thermally stimulated reactions is traditionally expected to produce an adequate kinetic description of the process in terms of the reaction model and of the Arrhenius parameters using a single-step kinetic equation

$$\frac{dX}{dt} = k(T)\, f(X) \qquad (9)$$

where t is the time, T is the temperature, X is the extent of conversion and $f(X)$ is the reaction model. In equation (9), $k(T)$ is the Arrhenius rate constant, which is given as:

$$k(T) = A\exp\left(\frac{-E}{RT}\right) \qquad (10)$$

where R is the gas constant, and A and E are Arrhenius parameters, the pre-exponential factor and the activation energy, respectively. For reaction kinetics under isothermal conditions, equation (9) can be analytically integrated to yield:

$$g(X) = \int_0^X \frac{dX}{f(X)} = k(T)t \qquad (11)$$

where $g(X)$ is the integral form of the reaction model.

Model evaluation

In order to apply the model-fitting method, the cited mathematical integral expressions $g(X)$ (Table 2) together with the experimental X and t values for given temperature, were inserted in equation (11). If one of the reaction models presented in Table 2 fit the experimental data, it will result in a straight line with the slope of k. That is, the values of kinetic rate constant, k, can be determined at different temperatures from slope of the straight line obtained by plotting $g(X)$ against time. This value can be subsequently inserted in the Arrhenius equation together with the corresponding temperature value to yield activation energy and pre-exponential factor values from the slope and intercept of regression straight-line. As illustrated by Figure 6, none of the expressions listed in Table 2 describe the kinetic complexity, in other word, none of the fitting model provide a straight line.

As an alternative, one can use another class of computational methods, which allow kinetic evaluations to be made without making any assumptions about the analytical form of the reaction model[34]. This class involves so-called isoconversional methods [34], which yield the activation energy as a function of the extent of conversion.

From isothermal TGA curves, a set of temperature *T* and *t* values were obtained for fixed values of *X*. Substituting *k=A exp(- E/RT)* in equation (11) one can obtains;

$$g(X) = A\exp\left(\frac{-E}{RT}\right)t \qquad (12)$$

By taking the logarithm and rearranging it, one can obtain;

$$\ln t = (-\ln A + \ln g(X)) + \frac{E}{RT} \qquad (13)$$

By plotting ln *t* versus *1/T* according to equation 13, the activation energies were found at any given *X* values from the slope of a regression line. Knowledge of the dependence activation energy on X assists in both detecting multi-step processes and drawing certain mechanistic conclusions[34]. Figure 7 provides the results of the model-free isoconversional computations using 20% CH_4 concentration. The activation energy varied between 36 kJ/mole and 56 kJ/mole for the conversion ranging from 0.1 to 0.5. The observed dependences suggest the occurrence of a multi-step process[35] that includes single steps with the estimated values of the activation energy between 36 and 56 kJ/mole. Vyazovkin and Linert[36] have shown that the decreasing dependence of activation energy on X corresponds to the kinetic scheme of a reversible reaction followed by an irreversible one.

Reaction Schemes

From these results it can be observed that the reaction of hematite with CH_4 follow multi-step kinetics. In this study, we have chosen a simple multi-step process that involves two parallel or series independent reactions.

$$\begin{aligned} A &\xrightarrow{k_1(T)} B \\ C &\xrightarrow{k_2(T)} D \end{aligned} \qquad (14)$$

While simple, this mechanism may reasonably approximate the process of conversion of a substance that exist in two isomeric forms, or a conversion of a reactant that simultaneously exists in two phases or a conversion of a solid by two separate paths to different products. As Figure 7 indicated that the activation energy decreases as conversion increases. The decreasing trend of activation energy in the multi steps of the reduction can be explain in the terms of a nucleation and growth model of reduction in which activation energy required during nucleation is higher than that needed in the growth stage[37]. Therefore, in this study it was assumed that both reactions follow the nucleation reaction model. The equations involved in isothermal processes are the following:

• Parallel:

$$\frac{X_t}{X_\infty} = w_1(1-e^{-a_1 t^{n_1}}) + w_2(1-e^{-a_2 t^{n_2}}) \qquad (15)$$

• Series:

$$\frac{X_t}{X_\infty} = w_1\left(\frac{1}{1-e^{-a_1 t^{n_1}}}\right) + w_2\left(\frac{1}{1-e^{-a_2 t^{n_2}}}\right) \qquad (16)$$

Where:
a_1=nucleation rate constant for the first mechanism (min.$^{-n_1}$),
a_2=nucleation rate constant for the second mechanism (min.$^{-n_2}$),
n_1= shape parameter for the first mechanism,
n_2= shape parameter for the second mechanism,
t=time (min),
w_1=weight factor for the first mechanism,
w_2= weight factor the second mechanism,
X_t=total conversion at any time t,
X_∞=equilibrium conversion.

For *n* values of 1, the equation (15) reduces to simple first order reaction kinetics. The equations (15) and (16) corresponds to two different nucleation or growth processes occurring in parallel or series, with the relative importance of each manifested by the value of the weight factors w_1 and w_2 where $w_1 + w_2 = 1$.[38] Note that equations (15) and (16) describe the isothermal processes, so *a*(T) is a constant at a given temperature. As illustrated by Figure 8, reaction model in series did not produce satisfactory results when compared to experimental data.

In nucleation and crystallization kinetic analyses, the "*a*" terms are described as a cluster of numerical and growth constants which are different in each reaction and the "*n*" terms are considered the kinetic exponent. As *a* decreases, the slope of the curve increases and takes a longer time to reach steady-state. As *n* increases, the conversion curve becomes steeper. According to diffusion controlled nucleation and growth theory, the magnitude of the shape factor, the "*n*" terms, reflects how the nucleation rate changes under isothermal conditions: 1.5 is a zero nucleation rate, 1.5 to 2.5 is a decreasing nucleation rate, 2.5 is a constant nucleation rate, and *n* values are greater than 2.5 for increasing nucleation rates.[39]

For a given temperature, values of X_∞, w_2, a_1, a_2 , $n_1$and $n_2$were determined by curve fitting the rate data of Figure 3 with the parameters in equation (15) using TABLECURVE available from Statistical Package for the Social Sciences. The values determined for the shape parameters, n_1, range from 0.8 to 1.4 for all the temperatures and all the CH_4 concentrations; the average value of n_1 was 1.01± 0.2 (95% CL). The values determined for the shape parameters, n_2, range from 1.57 to 3.1for all the temperatures and all the CH_4 concentrations; the average value of n_2 was 2.21± 0.4 (95%

CL) (see Table 3). The observed value of n_1= 1.01 was very close to the value of n_1= 1 that defines the pseudo-first order rate expression. In order to simplify the analysis, value of n_1= 1 was used. The values of X_∞, w_2, a_1, a_2 , and $n_2$were recalculated based on the approximation of n_1= 1 for every set of conversion data at different temperatures and CH_4 concentrations. The values determined for the shape parameters, n_2, range from 1.37 to 2.8 for all the temperatures and CH_4 concentrations with an average value of 2.17± 0.44 (95% CL) (see Table 3). The value of n_2= 2.17 is relatively close to the value of n_2= 2 that defines the Rayleigh distribution. The Rayleigh distribution is a special case for modeling the lifetime of a device that has a linearly increasing instantaneous failure rate. In order to simplify further analysis, a value of n_2= 2 was used. The values of X_∞, w_2, a_1, and a_2, were recalculated based on the approximation of n_1= 1 and n_2= 2 for every set of conversion data taken at different temperatures and CH_4 concentrations (see Table 3).

The effect of reaction temperature on the conversion of hematite during the 45 min reduction is shown in Figure 3. It should be noted the final mass (m_f) corresponding to conversion value of 1 was considered as mass of FeO. Increasing the temperature increased the reaction rate. It is clear from Figure 3 that the reduction developed over three phases. The first phase is mainly during the reduction of trivalent iron, second phase which consider as the main linear phase, and finally third phase started when the curve leveled off. It should be noted that the slope of the reduction curve represented the various reduction rates.

The comparison of the experimental hematite conversion data (X) and the conversion based on parallel model as presented in equation (15) (using n_1=1, and n_2=2) is illustrated in Figure 3 at different temperatures. The model data and experimental data agree over the entire conversion time with overall variance (R^2) greater than 99.9%. When fitting non-linear equations with a large number of parameters, it is prudent to consider how sensitive the trend is to the choice of input parameters, and whether equally good fits could be achieved with different sets of parameters. Indeed, it was found out the unknown parameters did not vary with different initial choices. The data in Figure 3 also shows that the rate of reduction of hematite increases as the reaction temperature is increased.

The parallel reactions, R_1 and R_2, based on model and experimental data are illustrated in Figure 9. The R_1 which is first order curve and R_2 which is sigmoidal curve represent two processes of reactions occurring simultaneously, but with different time dependence. The curve R_2 which represents reaction 2 has a faster time response than reaction 1 (curve R_1), and curve 3 is the sum of the two reactions R_1 and R_2. As time progresses, reaction 1 and 2 reach steady state at different degrees of reduction. That is, if process 1 alone were contributing to the bulk reaction, at long times the degree of reduction would be product of $w_1$and X_∞. With both reactions contributing, the degree of reduction at long times is product of (w_1+w_2) and X_∞. Figure 9 illustrates that in the initial portion of the reaction, the time dependence of total reaction, curves (R_1+R_2), and is dominated by reaction R_2. At long times, the total reaction (R_1+R_2) is dominated by reaction R_1. Hence, the reaction 1 will have little influence on the initial part of the reduction process.

The effects of reaction temperature on the conversion of each reaction (R_1 and R_2) during the 45 min reduction are shown in Figure 10. The data indicates that the reaction rates of both reactions R_1 and R_2 increases with increasing temperature. The difference in the final conversion of R2 indicated that there is unreacted Fe_2O_3 in the particles, likely being in the core regions of grains within the particles.

In order to determine the rate controlling mechanism, the value of apparent activation energy was calculated from Arrhenius equation as a function of Avrami kinetic constant (*a*);

$$k = a^{1/n} = k_0 e^{\frac{-E}{RT}} \qquad (14)$$

Where *k* is the reduction rate constant, k_0 is the frequency factor, *R* is the gas constant and T is the absolute temperature. The linear regression of the experimental data of ln *k* against 1/T determines *E/R*. A plot of *ln k* vs 1/T for reduction of hematite for both R_1 and R_2 are shown in Figure 11 at different reaction temperatures for all inlet CH_4 concentrations (15, 20, and 35%). The error bars lengths are defined by the range of the data at each temperature. The pre-exponential factor, k_0, and activation energy, *E*, were obtained from the intercept and slope of the straight line of *ln k* vs 1/T for a given CH_4 concentration. The apparent activation energies for both reactions R_1 and R_2 were estimated to be 34.4 ± 0.5 and 39.3 ± 1.5 kJ/mole respectively.

These activation energies are comparable with values obtained by other investigators.[31, 32] Abad et al.,[31] who studied the reaction rate of methane combustion over Fe45Al-FG found a value of 49 kJ/mole. Moghtaderi and Song[32] reported activation energy of 53 kJ/mole for reduction of iron ore with CH_4.

The values of shape factor indicate that as CH_4 concentration increases the value of w_2 also increases linearly. However, as temperature increases, the value of w_2 decreases linearly. A linear fit to the functionality gave a R^2 of greater than 85%. Combining all the values of w_2 for different temperatures and CH_4 concentrations, the following equation is obtained;

$$w_2 = 0.7953 - .000644 \times T(^oC) + 0.5443 \times y_{CH_4} \qquad (18)$$

The equilibrium conversion, X_∞, for all the CH_4 concentrations as a function of reaction temperatures indicates that the value of X_∞ increases linearly with increase in both concentrations and temperatures. A linear fit to the functionality gave a R^2 of greater than 82%. Combining all the values of X_∞ for different temperatures and CH_4 concentrations, the following equation is obtained;

$$X_\infty = -1.374 + .00237 \times T(^oC) + 0.6624 \times y_{CH_4} \qquad (19)$$

An expression for the reaction rate, *dX/dt*; can be derived by differentiating equation (15) with respect to t, at constant temperature, as follows:

$$\frac{dX_1}{dt}\Big|_{R_1} = a_1\left(w_1 X_\infty - X_1\right) \tag{20}$$

and

$$\frac{dX_2}{dt}\Big|_{R_2} = n a_2^{\frac{1}{n}}\left(w_2 X_\infty - X_2\right)\left(-\ln(1-\frac{X_2}{w_2 X_\infty})\right)^{(1-\frac{1}{n})} \tag{21}$$

Therefore, the total rate is summation of equations (20) and (21) as;

$$\frac{dX_t}{dt}\Big|_{R_1+R_2} = a_1\left(w_1 X_\infty - X_1\right) + n a_2^{\frac{1}{n}}\left(w_2 X_\infty - X_2\right)\left(-\ln(1-\frac{X_2}{w_2 X_\infty})\right)^{(1-\frac{1}{n})} \tag{22}$$

The value of *n* depends on the shape of the nuclei and the dimensionality of their growth, as well as on the rate of their formation[40]. When nucleation sites are instantaneously formed, *n* has the value of 1 for needle-shaped crystals, 2 for plates, and 3 for spheres. If additional nucleation sites sporadically appear with time, the value for *n* is one integer higher. Most polymer crystals are anticipated to be spherical in nature, so values of *n* between 3 and 4 are most common. However, as stated earlier, a value of *n*=2 was chosen for Eq. (21) consistent with the formation of platelets.
Combining all the values of k_1 and k_2 for different CH_4 concentrations and placing them in Eq. 14, the following global *k*'s equation were obtained

$$k_1 = a_1 = 4.759\, y_{CH_4}^{0.636} e^{\frac{-4134.2}{T}} \tag{23}$$

and

$$k_2 = a_2^{1/2} = 133\, y_{CH_4}^{1.06} e^{\frac{-4731.2}{T}} \tag{24}$$

The coefficients were taken as the average of the upper and lower limits for 95% confidence limits.
The rate−time (dX/dt vs t) data obtained at different temperatures (700−825 ^{o}C) using Eq. (22) are shown in Figure 12. The individual rate-time data obtained at different temperatures (700−825 °C) using equations (20) and (21) are also shown in Figures 13 and 14 for reactions R_1 and R_2. As shown in Figure 13, the rate−time curves for R_1 shows that the maximum rate when times equal to zero at all temperatures. This is consistent with rate data of kinetically controlled reaction in which the maximum rate occurs when time equal to 0, or when *n* equal to 1 in the Avarami equation. However, as shown in Figure 14, the rate−time curves for R_2 show that the maximum rate at a time greater than 0 which indicates that R_2 is not a kinetically controlled reaction. Also, it shows that the rate at time equal to zero is zero, thus R_1 leads R_2. Data in Figures 13 and 14 also show that the value of maximum rate increases with the increasing temperature for both R_1 and R_2.

Figure 15 shows the product gas concentration (as measured by mass spectrometer) variation as a function of time at the reaction temperature of 825 ^{o}C. The data in Figure 15 also shows that the CH_4 concentration at the outlet increases rapidly reaches a temporat maxima, decreases slightly and then increases to the final value. The temporal maxima is reached at the same time that the CO_2 begins to increase. Then CH_4 concentrations continue to increase simultaneously with H_2 then reach a maximum value. Figure 16 shows the CO_2 and H_2O concentrations (since there was no calibration data for H_2O concentration, Figure 16 shows Ion concentration for H_2O and CO_2) reach their maximum value initially when CH_4 concentration was still increasing indicating that most of the CH_4 was totally oxidized into CO_2 and H_2O at the early stages of the reduction period. As the reaction proceeded, the remaining unconverted CH_4 was detected. At the same time, a minor amount of CO and H_2 were released due to partially oxidization of some CH_4 to CO and H_2 instead of CO_2 and H_2O.

One of the goals of kinetic studies is to deduce the reaction mechanism. As apparent from Figure 7 that activation energy decreases with increasing conversion. In our case, the reduction of hematite to magnetite probably proceeds through the exothermic stage at low conversion, which resulted in high activation energy.[35] The initial high activation energy represent the sum of the enthalpy of reversible process and of the activation energy of the irreversible process. On the other hand, lower value of the activation energy at the higher conversion is a characteristic of the process proceeding through a reversible endothermic process.[35]

The possible reaction mechanism is summarized below.

Methane decomposition and reduction of hematite to Fe_3O_4

$$3CH_4 \rightarrow 3C + 6H_2 \qquad \Delta H^o_{r,800C} = 268.34\,kJ/mol \quad (25)$$

$$CH_4 + 12Fe_2O_3 \rightarrow 8Fe_3O_4 + CO_2 + 2H_2O \qquad \Delta H^o_{r,800C} = 164.1\,kJ/mol \quad (26)$$

$$3C + 12Fe_2O_3 \rightarrow 8Fe_3O_4 + CO_2 + 2CO \qquad \Delta H^o_{r,800C} = 346.2\,kJ/mol \quad (27)$$

$$H_2 + 3Fe_2O_3 \rightarrow 2Fe_3O_4 + H_2O \qquad \Delta H^o_{r,800C} = -6.75\,kJ/mol \quad (28)$$

$$4CH_4 + 27Fe_2O_3 \rightarrow 18Fe_3O_4 + 2CO_2 + 2CO + 3H_2O + 5H_2 \qquad \Delta H^o_{r,800C} = 771.86\,kJ/mol \quad (R_2) \quad (29)$$

Methane decomposition and reduction of Fe_3O_4 to FeO

$$2CH_4 \rightarrow 2C + 4H_2 \qquad \Delta H^o_{r,800C} = 178.9\,kJ/mol \quad (30)$$

$$CH_4 + 4Fe_3O_4 \rightarrow 3FeO + 2H_2O + CO_2 \qquad \Delta H^o_{r,800C} = 377.9\,kJ/mol \quad (31)$$

$$2C + 3Fe_3O_4 \rightarrow 9FeO + CO_2 + CO \qquad \Delta H^o_{r,800C} = 377.5\,kJ/mol \quad (32)$$

$$H_2 + Fe_3O_4 \rightarrow 3FeO + H_2O \qquad \Delta H^o_{r,800C} = 46\,kJ/mol \quad (33)$$

$$3CH_4 + 8Fe_3O_4 \rightarrow 24FeO + 2CO_2 + CO + 3H_2O + 3H_2 \qquad \Delta H^o_{r,800C} = 981\,kJ/mol \quad (34)$$

(R_1)

$$7CH_4 + 27Fe_2O_3 \rightarrow 10Fe_3O_4 + 24FeO + 4CO_2 + 3CO + 6H_2O + 8H_2$$

$$\Delta H^{o}_{r,800C} = 1752.9\, kJ/mol \qquad (35)$$

It is significant that the mass spectrometry detection of CH_4 and H_2 were observed initially during the hematite reduction. The observation of CO and H_2 indicates that the reactive gas (CH_4) initiates hematite reduction.
These results suggest that the reduction of hematite (Fe_2O_3) to be initially control by the topochemical process. Once a thin layer of lower iron oxides (wüsite) is formed on the surface; then the mechanism shifts to two simultaneous reaction mechanism (Fe_2O_3 to FeO and produce CO and H_2 , intrinsic topochemical kinetics and Fe_2O_3 to Fe_3O_4 and produce CO_2 and H_2O, nucleation and growth kinetics).

Figure 17 illustrates the comparison of rate of R_2 versus time at 825 °C, and the H_2O and CO_2 concentration, as measured by the mass spectrometer at the outlet of TGA. The shape of the H_2O and CO_2 concentrations curve with time is very similar to the shape of rate versus time data for R_2. This confirms the validity of the Avarmi model for reaction R_2 (equation 21). As also shown in Figure 10, the final conversion products in R_2 at 825 ^{o}C correspond to Fe_3O_4 which is consistent with reaction R_2.
It should be noted that, Figure 10 also shows that the conversion of R_1 produces a mixture of FeO and Fe_3O_4.

Conclusion

In this study, a rigorous approach has been taken to describe the kinetics of the reduction of hematite in methane atmosphere over the range of 700–825 ^{o}C and three CH_4 concentrations: 15, 20, and 35%. Experimental results suggested that, within the range of temperatures studied, the kinetics of reduction of hematite involve two competing reaction process. The first expression provided a 1st order kinetics rate; whereas the second expression provided a nucleation and growth process with an Avrami's exponent of n=2. These results suggest that the reduction of hematite (Fe_2O_3) proceed via a two simultaneous steps mechanism. Activation energies and pre-exponential factors were measured for the rate constants of both reactions. The activation energy value evaluated are 39.3 ± 1.6 kJ/mole for reaction of R_2 and 34.4 ± 0.5 kJ/mole for reaction of R_1. The reaction rates for both reaction increases as temperature was increased. The experimental results suggested that the Iron oxide is an ideal candidate as an oxygen carrier for CLC system burning methane.

Acknowledgment

The authors acknowledge the Department of Energy for funding the research through the office of Fossil Energy's Gasification Technology and Advanced Research funding programs. Special thanks go to Hanjing Tian and Thomas Simonyi of URS Energy & Construction, Inc. for their assistance with experimental work and data.

DISCLAIMER

The U.S. Department of Energy, NETL and ADA-ES contributions to this report was prepared as an account of work sponsored by an agency of the United States Government. Neither the United States Government nor any agency thereof, nor any of their employees, makes any warranty, express or implied, or assumes any legal liability or responsibility for the accuracy, completeness, or usefulness of any information, apparatus, product, or process disclosed, or represents that its use would not infringe privately owned rights. Reference herein to any specific commercial product, process, or service by trade name, trademark, manufacturer, or otherwise does not necessarily constitute or imply its endorsement, recommendation, or favoring by the United States Government or any agency thereof. The views and opinions of authors expressed herein do not necessarily state or reflect those of the United States Government or any agency thereof.

The authors declare no competing financial interest.

References

[1] P. Cho,, T. Mattisson, A. Lyngfelt, Defluidization conditions for a fluidized bed of iron oxide-, nickel oxide-, and manganese oxide-containing oxygen carriers for chemical looping combustion, Industrial and Engineering ChemistryResearch 45 (2006**)** 968–977.

[2] H. Fang, L. Haibin, Z. Zengli, Advancements in Development of Chemical-Looping Combustion: A Review, International Journal of Chemical Engineering (2009), Article ID 710515, 16 pages, doi:10.1155/2009/710515

[3] M. Akai, T. Kagajo, M. Inoue, Performance Evaluation of Fossil Power Plant with CO_2 Recovery and a Sequestering System, *Energy Convers. Mgmt*, 36 (1995) 801-804.

[4] N. Kimura, K. Omata, T. Kiga, S. Takano, S. Shikisma, The Characteristics of pulverized coal combustion in O_2/CO_2 mixtures for CO_2 recovery: Energy Convers. Mgmt. 36 (1995) 805-808.

[5] M. Ishida, H. Jin, CO_2 recovery in a power plant with chemical looping combustion Energy Convers. Mgmt. 38 (1996) 187-192.

[6] H.J. Richter, K.F. Knoche, Reversibility of combustion processes, ACS Symposium Series, 235 (1983) 71-85.

[7] M. Ishida, D. Zheng, T. Akehata, Evaluation of a chemical-looping-combustion power-generation system by graphic exergy analysis, Energy-The Int. Journal, 12 (1987) 147-154.

[8] W.G. Xiang, Y.Y. Chen, Hydrogen and electricity from coal with carbon dioxide separation using chemical looping reactors, Energy Fuels 21 (2007) 2272–2277.

[9] P. Gupta, L.G. Velazquez-Vargas, L.S. Fan, Syngas Redox (SGR) Process to Produce Hydrogen from Coal Derived Syngas, Energy Fuels 21 (2007) 2900–2908.
[10] P. Chiesa, G. Lozza, A. Malandrino, M. Romano, V. Piccolo, Three-reactors chemical looping process for hydrogen production, Int. J. Hydrogen Energy 33 (2008) 2233–2245.
[11] J. Adánez, L.F. de Diego, F. García-Labiano, P. Gayán, A. Abad, Selection of oxygen carriers for chemical-looping combustion, Energy Fuels 18 (2004) 371–377.
[13] H.-J. Ryu, D.-H. Bae, K.-H. Han, S.-Y. Lee, G.-T. Jin, J.-H. Choi, Oxidation and Reduction Characteristics of Oxygen Carrier Particles and Reaction Kinetics by Unreacted Core Model, Korean J. Chem. Eng. 18 (2001) 831−837.
[14] H.-J. Ryu, D.-H. Bae, G,-T. Jin, Effect of Temperature on Reduction Reactivity of Oxygen Carrier Particles in a Fixed Bed Chemical-Looping Combustor, Korean J. Chem. Eng. 20 (2003) 960−966.
[15] Y. Nakano, S. Iwamoto, T. Maeda, M. Ishida, T. Akehata, Characteristics of Reduction and Oxidation Cycle Process by use of a Fe_2O_3 Medium, Iron Steel J. Jpn. 72 (1986) 1521−1528.

[17] M. Ishida, H. J. Jin, A Novel Combustor Based on Chemical-looping Reactions and its Reaction Kinetics, Chem. Eng. Jpn. 27 (1994) 296−301.
[18] M. Ishida, H. Jin, Novel Chemical-looping Combustor without NOx Formation, Ind. Eng. Chem. Res. 35 (1996) 2469−2472.
[19] H. Jin, T.Okamoto, M. Ishida, Development of a Novel Chemical-Looping Combustion: Synthesis of a Looping Material with a Double Metal Oxide of CoO-NiO, Energy Fuels 12 (1998) 1272−1277.
[20] H. Jin, T. Okamoto, M. Ishida, Development of a Novel Chemical looping Combustion: Synthesis of a Solid Looping Material of NiONiAl2O4, Ind. Eng. Chem. Res. 38 (1999) 126−132.
[21] H. Jin, M. Ishida, Reactivity Study on Natural-gas-fueled Chemical looping Combustion by a Fixed Bed, Ind. Eng. Chem. Res. 41 (2002) 4004−4007.
[22] R. J. Copeland, G. Alptekin, M. Cesario, S. Gebhard, Y. Gershanovich, A Novel CO_2 Separation System. 8th International Symposium on Transport Phenomena and Dynamics of Rotating Machinery, Honolulu, HI, 2000.
[23] R. J. Copeland, G. Alptekin, M. Cessario, Y. Gerhanovich, A Novel CO_2 Separation System. Proceedings of the First National Conference on Carbon Sequestration, DOE/NETL, Washington, DC, 2001; LA-UR-00-1850.
[24] A. A. Scott, J. S. Dennis, A. N. Hayhurst, T. Brown, In situ gasification of a solid fuel and CO_2 separation using chemical looping, AIChE J. 52 (2006) 3325-3328.
[25] J. R. Scheffe, M. D. Allendorf, E. N. Coker, B. W. Jacobs, A. H. McDaniel, A. W. Weimer, Chemistry of Materials 23 (2011) 2030-2038.
[26] M. M. Hossain, K. E. Sedor, H. I. de Lasa, Co-Ni/Al2O3oxygen carrier for fluidized bed chemical-looping combustion: desorption kinetics and metal-support interaction, Chem. Eng. Sci. 62 (2007**)** 5464–5472.
[27] J. Bessieres, A. Bessieres, J. J. Heizmann, Iron oxide reduction kinetics by hydrogen, Int. J. Hydrogen Energy 5 (1980) 585-595.
[28] A.A. El-Geassy, K.A. Shehata, S.Y. Ezz, Mechanism of iron oxide reduction with hydrogen/carbon monoxide mixtures, Trans. ISIJ 17 (1977) 629-635.

[29] A.A.El-Geassy, M.I. Nasr, M.M. Hessien, Effect of reducing gas on the Volume Change during Reduction of Iron Oxide Compacts, ISIJ Int. 36 (1996) 640-649.
[30] K.S. Go, S. R. Son, S.D. Kim, Reaction kinetics of reduction and oxidation of metal oxides for hydrogen production, Int. J. Hydrogen Energy 33 (2008) 5986-5995.
[31] A. Abad, J. Adánez, F. García-Labiano, L. F. de Diego, P. Gayán, J. Celaya, Mapping of the range of operational conditions for Cu-, Fe-, and Ni-based oxygen carriers in chemical-looping combustion, Chemical Engineering Science 62 (2007) 533 – 549.
[32] B. Moghtaderi, H. Song Energy and Fuels 24 (2010) 5359–5368.
[33] D. Ghosh, A.K. Roy, A. Ghosh Transactions of the Iron and Steel Institute of Japan 26 (1986) 186-193.
[34] S. Vyazovkin, A unified approach to kinetic processing of nonisothermal data, Int. J. Chem. Kinet. 28 (1996) 95-101.
[35] S. Vyazovkin, Conversion dependence of activation energy for model DSC curves of consecutive reactions, Thermochim Acta. 236 (1994) 1-13.
[36] S. Vyazovkin, W. Linert, Kinetic analysis of reversible thermal decomposition of solids, Int. J. Chem. Kinet. 27 (1995) 73-84.
[37] P. Pourghahramani, E.Forssberg, Reduction kinetics of mechanically activated hematite concentrate with hydrogen gas using nonisothermal methods, Thermochima Acta. 454 (2007) 69-77.
[38] C. N. Velisaris, J. C. Sefeis, Crystallization kinetics of polyetheretherketone (PEEK) matrices, Polym. Eng. Sci. 26 (1986) 1574-1581.
[39] J. Málek, The applicability of Johnson-Mehl-Avrami model in the thermal analysis of the crystallization kinetics of glasses, Thermochim Acta. 267 (1995) 61–73.
[40] J. Sestak, Thermophysical Properties of Solids, Their Measurements and Theoretical Analysis, Elsevier, Amsterdam, (1984); p 190.

Table 1. Composition of hematite, wt%

C	O	Si	Mn	Fe	Ag	Au	Total
1.24	36.89	1.38	1.9	57.78	0.08	0.73	100

Table 2. Kinetic models for solid state reactions.

Kinetic Model	Kinetic mechanism	*f(X)*	*g(X)*
Kinetics-order models	1st order	$(1-X)$	$-ln(1-X)$
	2nd order	$(1-X)^2$	$(1-X)^{-1}-1$
	3rd order	$(1-X)^3$	$1/2[(1-X)^{-2}-1]$
Diffusion model	1-D	$1/(2X)$	X^2
	2-D	$1/[-ln(1-X)]$	$(1-X)ln(1-X)+X$
	3-D	$(3/2)(1-X)^{2/3}[1-(1-X)^{1/3}]$	$[1-(1-X)^{1/3}]^2$
Contraction Model	2-D	$2(1-X)^{1/2}$	$[1-(1-X)^{1/2}]$
	3-D	$3(1-X)^{2/3}$	$[1-(1-X)^{1/3}]$
Nucleation Model	variable n	$n(1-X)[-ln(1-X)]^{(1-1/n)}$	$[-ln(1-X)]^{(1/n)}$

Table 3. Parameters obtained by fitting Eq. (15) to experimental data for different temperatures and CH_4 concentrations. R^2 for all curve fits was greater than 0.999

	CH_4=35%				CH_4=20%				CH_4=15%		
T(^{0}C)	700	750	800	825	700	750	800	825	750	800	825
X_∞	0.524	0.583	0.808	1.000	0.311	0.565	0.638	0.746	0.330	0.489	0.623
w_1	0.492	0.565	0.625	0.638	0.563	0.577	0.621	0.679	0.582	0.581	0.646
a_1	0.068	0.071	0.085	0.085	0.039	0.049	0.042	0.051	0.020	0.023	0.025
n_1	0.831	0.802	0.796	0.791	1.132	1.012	0.937	0.923	1.248	1.133	1.111
a_2	0.057	0.109	0.292	0.325	0.036	0.038	0.122	0.134	0.016	0.039	0.048
n_2	2.518	2.346	1.788	1.568	2.319	2.441	1.946	1.962	2.392	2.102	2.078
					n_1=1						
X_∞	0.506	0.552	0.772	0.955	0.315	0.565	0.624	0.730	0.349	0.506	0.642
w_1	0.569	0.513	0.465	0.458	0.380	0.417	0.404	0.354	0.329	0.369	0.310
a_1	0.073	0.140	0.331	0.360	0.023	0.036	0.131	0.151	0.007	0.030	0.037
a_2	2.312	2.081	1.555	1.374	2.582	2.472	1.881	1.844	2.800	2.264	2.257
n_2	0.041	0.040	0.046	0.045	0.060	0.051	0.035	0.041	0.042	0.034	0.035
					n_1=1 n_2=2						
	700	750	800	825	700	750	800	825	750	800	825
X_∞	0.520	0.555	0.757	0.926	0.323	0.581	0.618	0.724	0.385	0.527	0.658
w_1	0.576	0.515	0.446	0.425	0.435	0.448	0.401	0.348	0.385	0.380	0.321
a_1	0.099	0.149	0.273	0.280	0.048	0.062	0.118	0.133	0.027	0.043	0.051
a_2	0.035	0.039	0.052	0.054	0.025	0.035	0.037	0.042	0.024	0.029	0.032

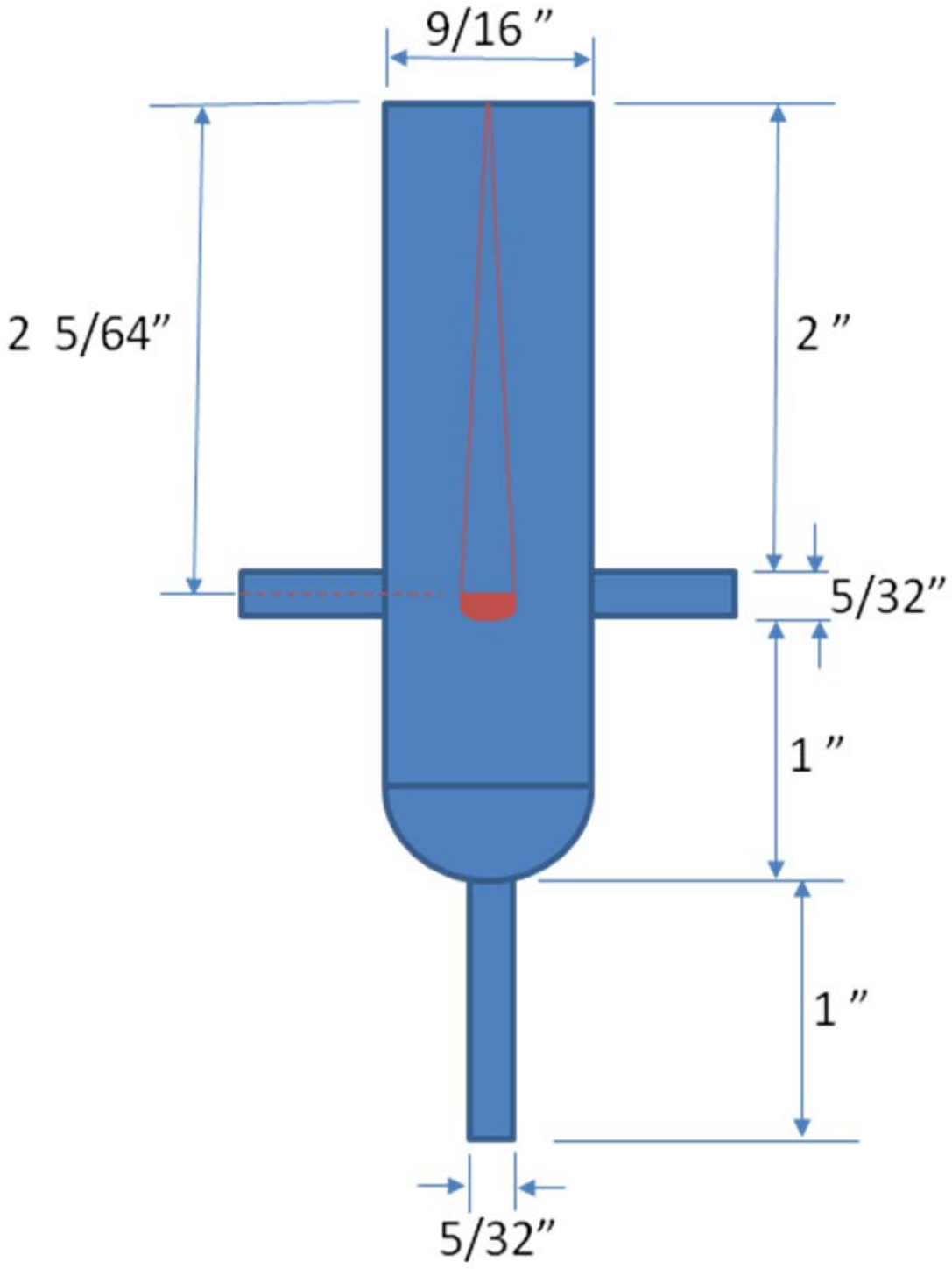

Figure 1 – Sketch of TA Model 2050 thermo gravimetric analyzer

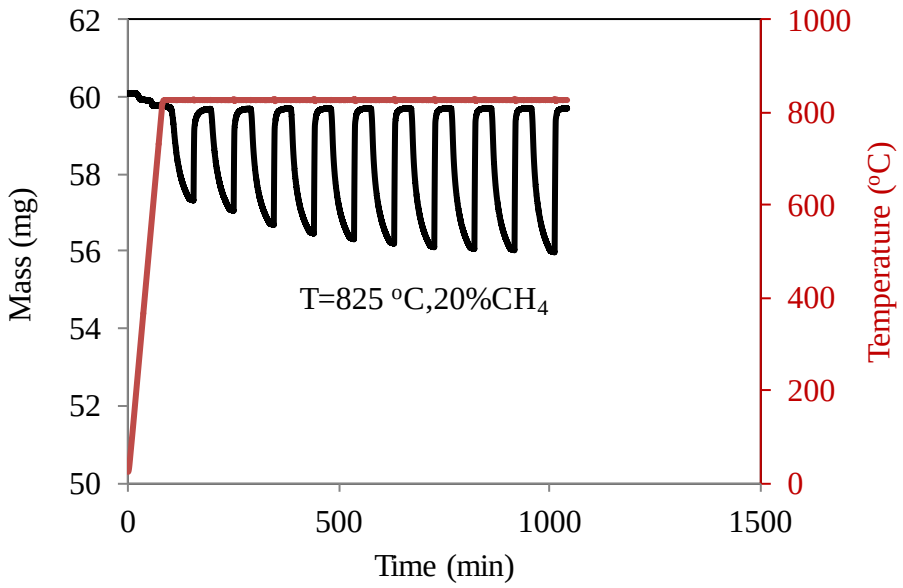

Figure 2. Typical mass and temperature measurement for hematite particle of 80 μm using 20% CH_4 for reduction and air for oxidation reactions.

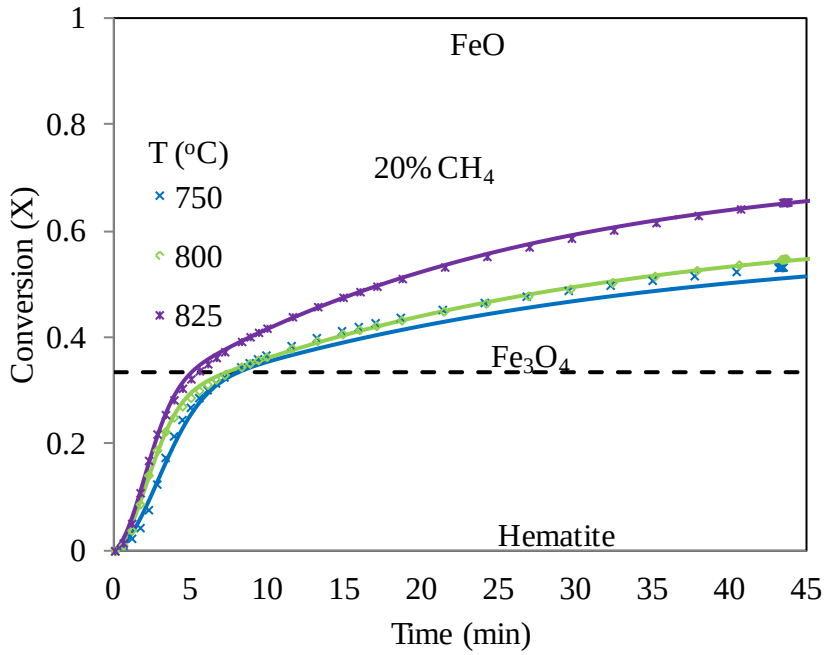

Figure 3. Effect of reaction temperature on conversion of Hematite to FeO using 20% CH_4.

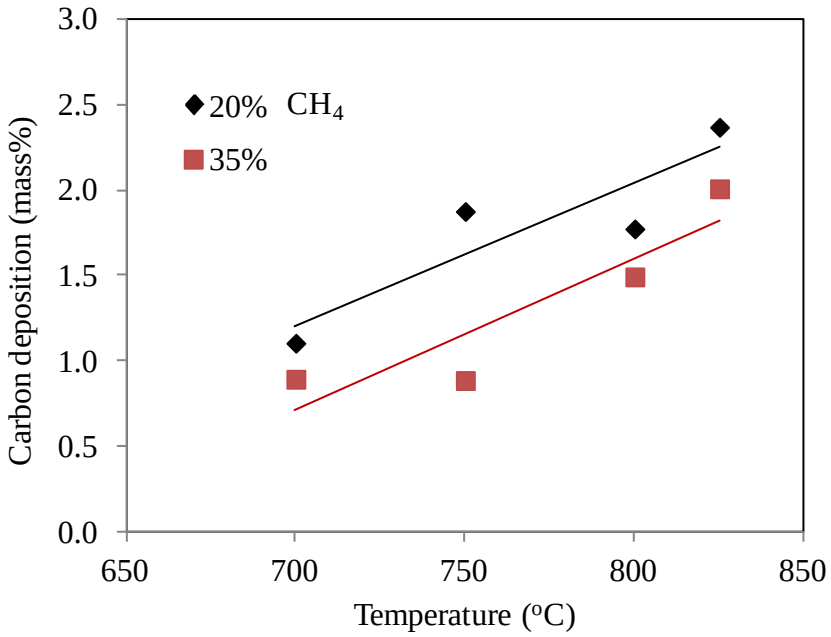

Figure 4. Carbon contents in reduced hematite for different temperature and CH_4 concentrations (20% and 35%).

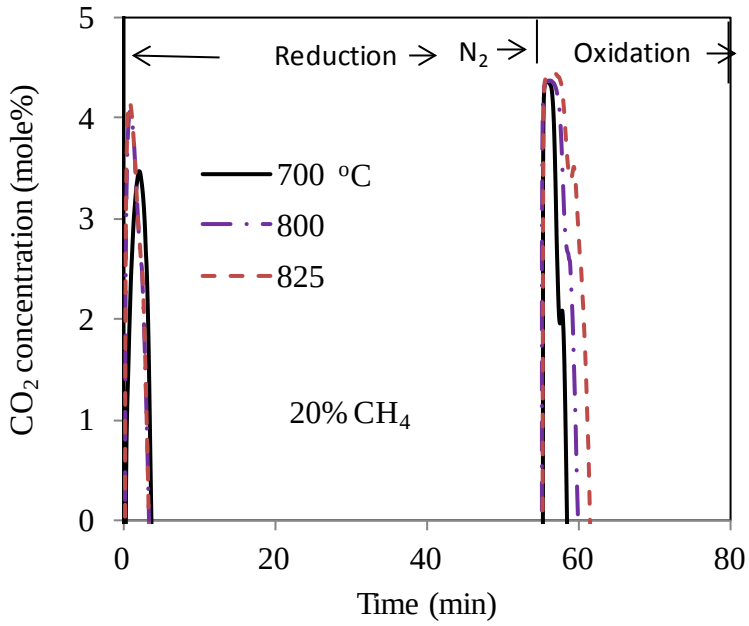

Figure 5. Effect of temperatures on CO_2 concentration during reduction and oxidation of hematite.

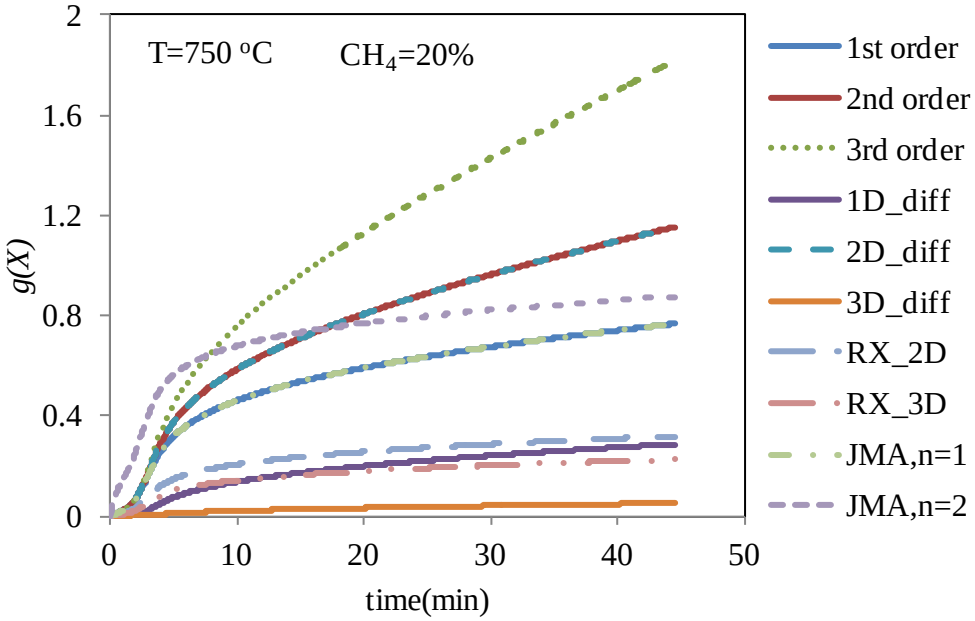

Figure 6. Examination of linear relationship for different reaction models.

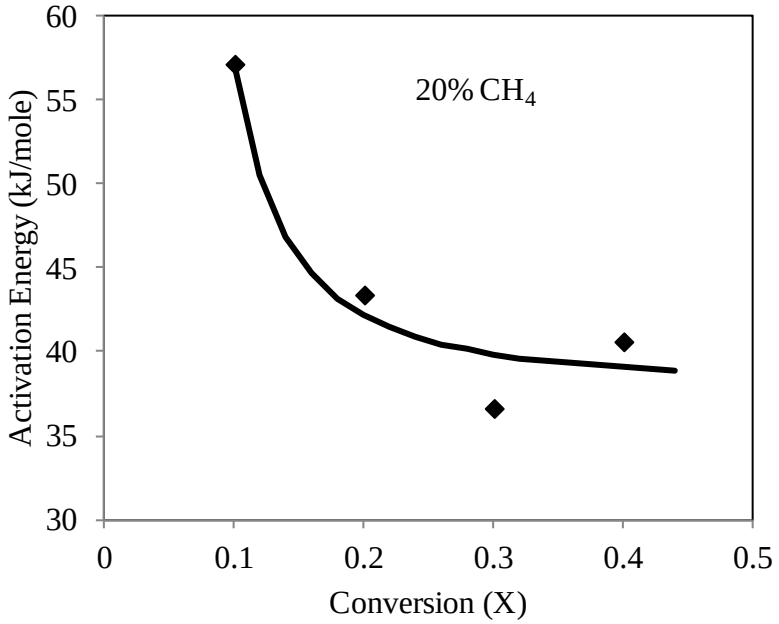

Figure 7. Activation energy values as a function of *X* obtained by an isothermal isoconversional method using 20% CH_4.

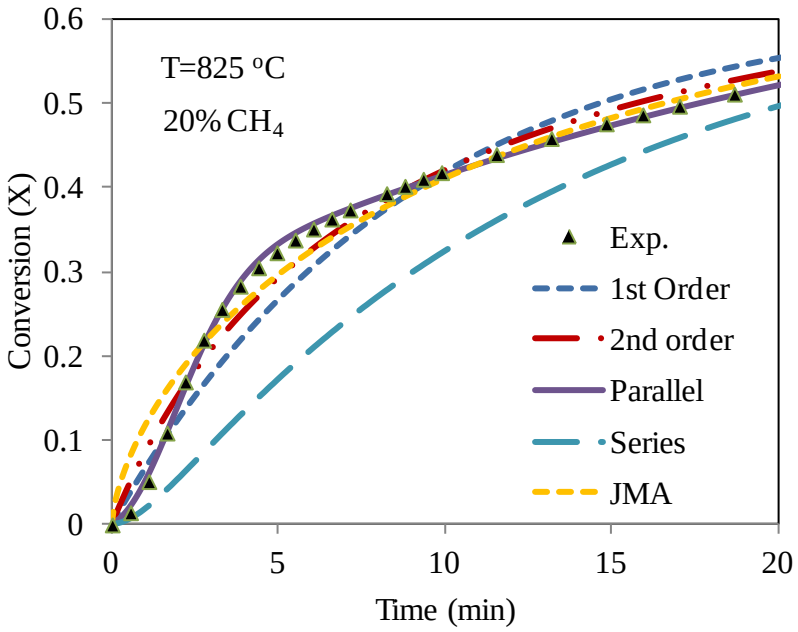

Figure 8. Curve fitting of experimental reduction data using first and second-order reaction rates, series and parallel reactions, and JMA rates for 20% methane and 825 °C.

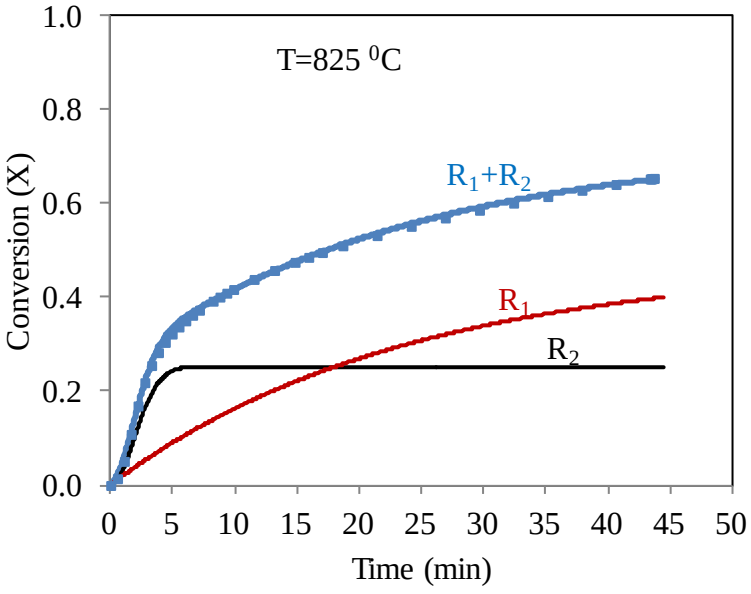

Figure 9. Three predicted curves of conversion as a function of time during isothermal reaction of Fe_2O_3 with 20% CH_4. Curve R_1: single 1st order reaction; curve R_2: single Avrami equation with n=2.0; curve R_1+R_2: parallel reaction representing the sum of curve R_1 and R_2. Doted points are experimental data.

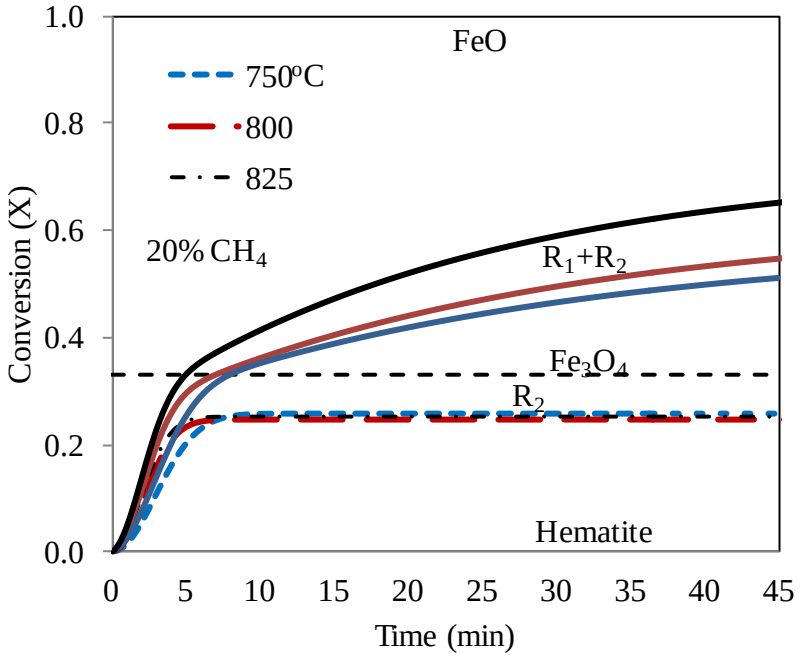

Figure 10. Effect of reaction temperature on conversion of R_1 and R_2 using 20% CH_4.

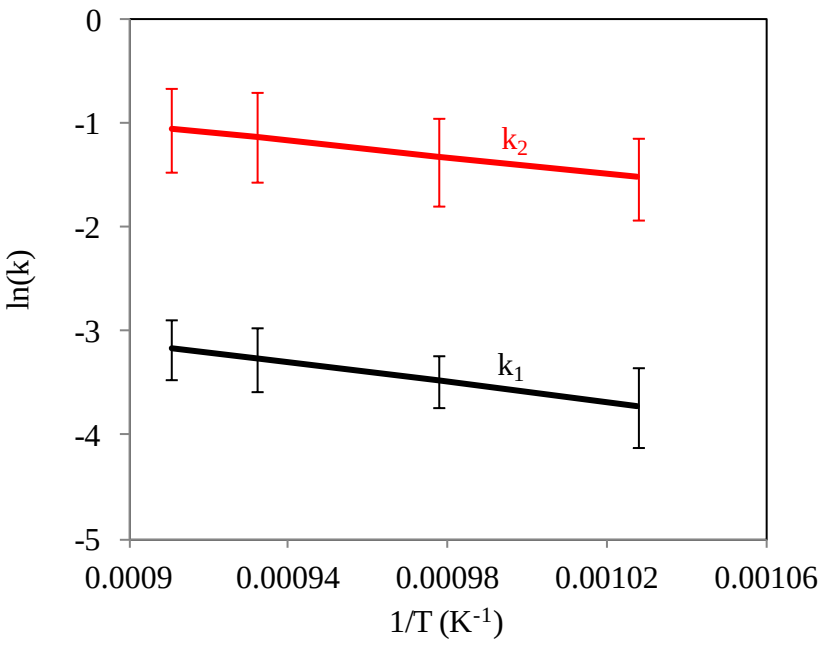

Figure 11. Temperature dependence of the reaction rate, k (min^{-1}), for two parallel reactions for all CH_4 concentrations. Error bars are defined by data range.

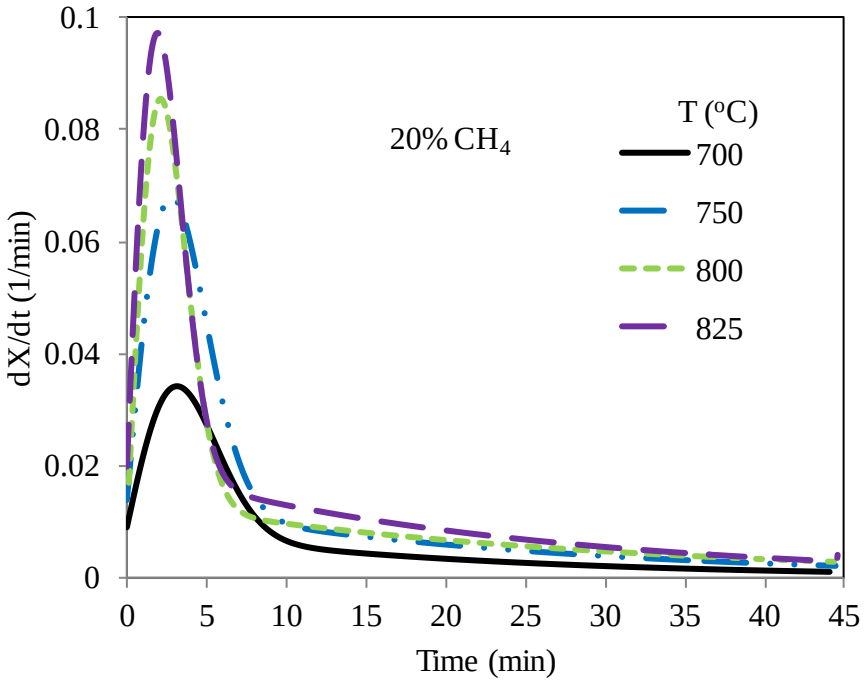

Figure 12. Effect of reaction temperature on the rate of reduction of hematite particle with 20% CH_4 reaction.

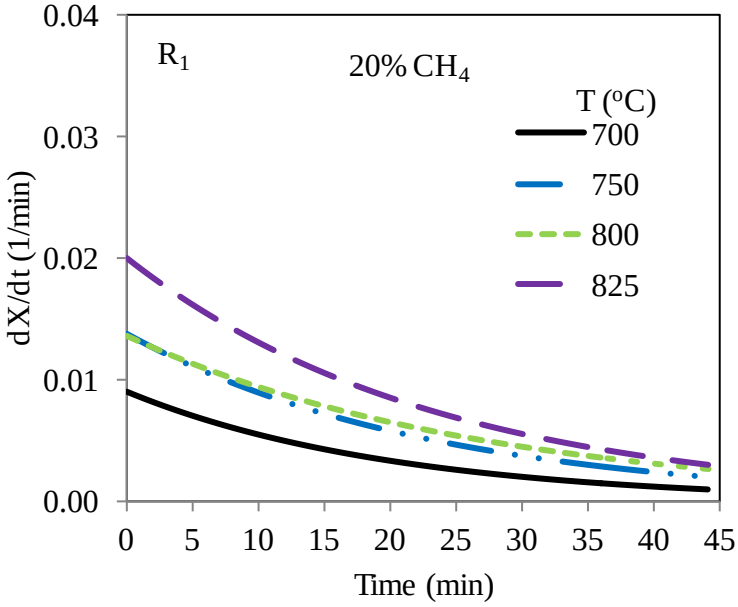

Figure 13. Effect of reaction temperature on the rate reduction of R_1 and CH_4 reaction.

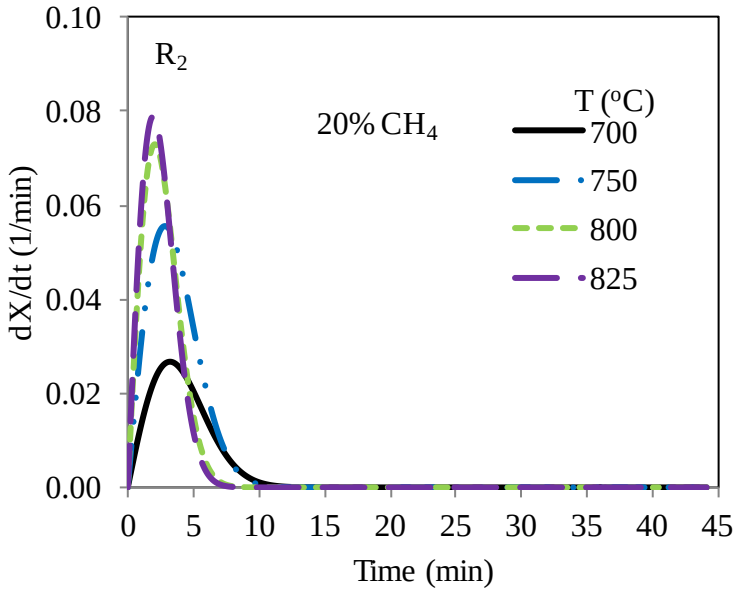

Figure 14. Effect of reaction temperature on the rate reduction of R_2 and CH_4 reaction.

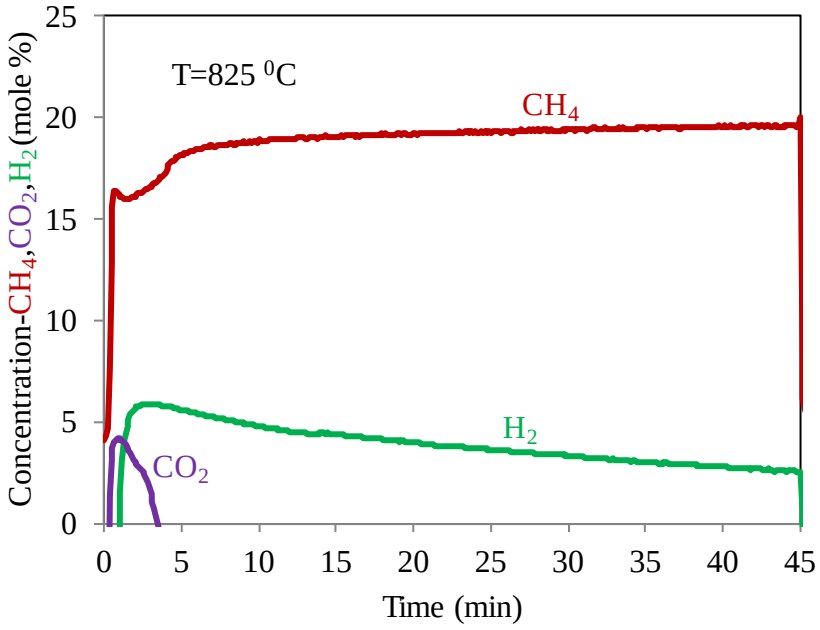

Figure 15. Outlet gas analysis for the reduction of Hematite (Fe_2O_3) with methane (20% CH_4) using a reaction temperature of 825 °C.

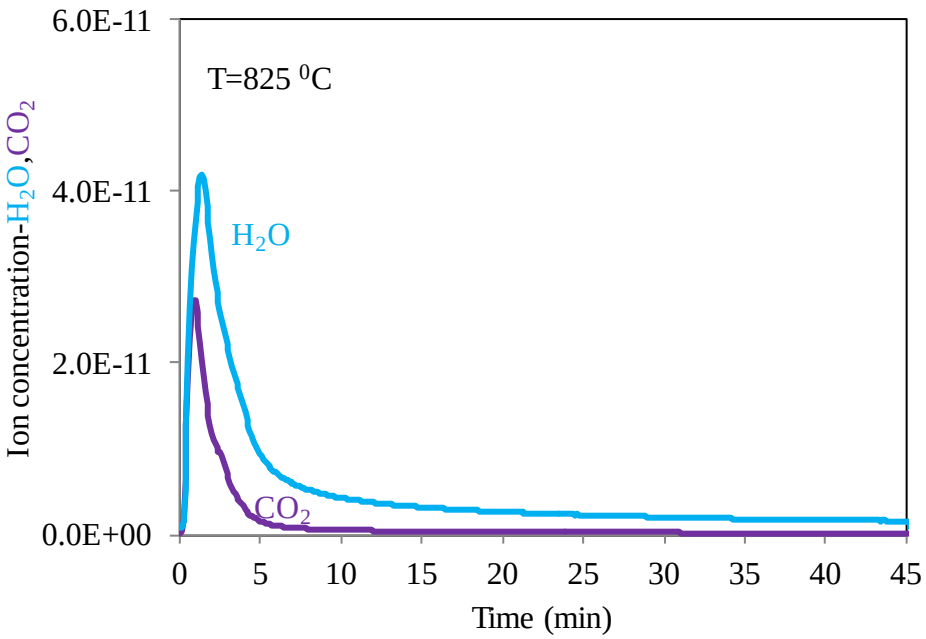

Figure 16. Ionic concentration of H_2O and CO_2 for the reduction of Hematite (Fe_2O_3) with methane (20% CH_4) using a reaction temperature of 825 °C.

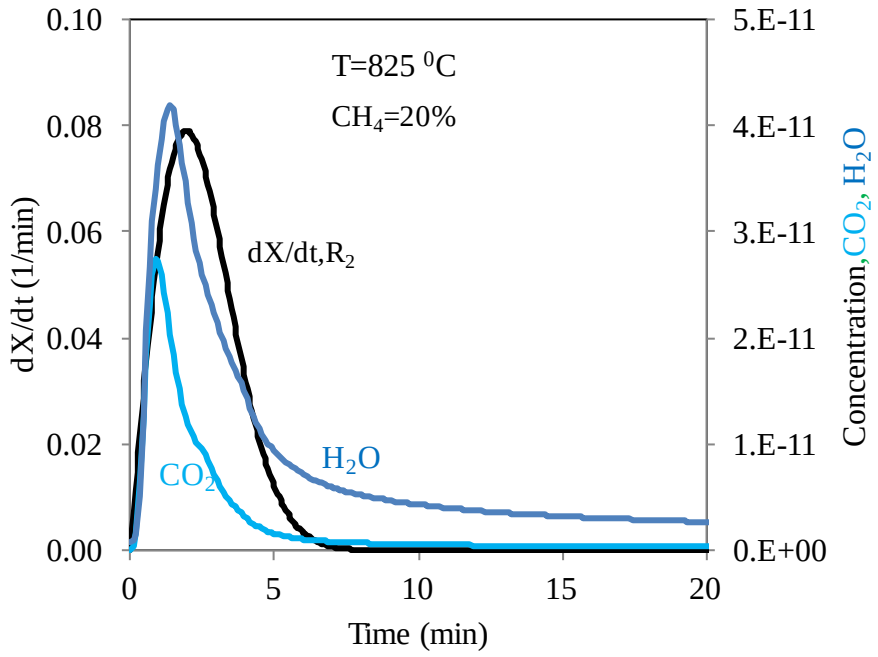

Figure 17. Similarity in the shape of the H_2O and CO_2 curve with time as compared to the conversion rate data (numerical derivative) of the TGA reduction data for reaction R_2.